

PETROPHYSICAL PARAMETERS AND ELECTROFACIES MODELS OF THE ITARARÉ GROUP APPLYING MULTI-RESOLUTION GRAPH-BASED CLUSTERING METHOD, PARANÁ BASIN

RUNNING TITLE: PETROPHYSICS AND ELECTROFACIES USING CLUSTERING METHOD

Marco Antônio R. de Almeida^{id}, Marivaldo dos Santos Nascimento^{id}, and
Marvim Francis Mota Alves^{id}

Universidade Federal de Santa Catarina - UFSC, Departamento de Geologia, Florianópolis, SC, Brazil

*Corresponding author email: mar.almeida@outlook.com

ABSTRACT. Volume shale (V_{sh}) and effective porosity (Φ_e) were calculated and partially applied as petrophysical input parameters to generate electrofacies models using the Multi-Resolution Graph-Based Clustering method in sedimentary successions of the Itararé Group. The petrophysical parameters and electrofacies models were determined from geophysical data from two wells located in the eastern portion of the Paraná Basin. The stratigraphic intervals in each well (analogues of hydrocarbon reservoirs) allowed petrophysical analysis and the determination of electrofacies models based on gamma ray profiles, apparent density and neutron porosity, together with lithological data. The petrophysical parameters were calculated by different procedures, and the effective porosity results were applied as input parameters for electrofacies modeling. The electrofacies models were correlated to lithological data and patterns of gamma ray profiles and apparent density, as well as different types of porosity. The generated models provide differences related to the type of porosity, the method applied to calculate the effective porosity and present probable relationships with the lithological units of the wells.

Keywords: volume shale; porosity; bulk-density; gamma ray; stratigraphy

INTRODUCTION

Petrophysical analysis is one of the most useful and important tools available for reservoir characterization as they help to define physical rock characteristics based on well log data. The

petrophysical analysis includes the determination of parameters such as lithology, volume shale, porosity, water saturation, hydrocarbon saturation, pore geometry, and permeability. Well log data are also used to identify productive zones, to determine depth and thickness of zones, to distinguish oil, gas, and water zones in a reservoir, and to estimate hydrocarbon reserves. Furthermore, geologic maps developed from log interpretation are useful in determining facies relationships and drilling locations (Asquith et al., 2004).

Electrofacies are unique combinations of petrophysical log responses that reflect specific physical and compositional characteristics of a rock interval cut by a borehole (Serra & Abbott, 1982; Sagar et al., 2018). Electrofacies characterization is widely used in petroleum prospecting, and it is an essential component for reservoir characterization. It involves partitioning a set of log data into electrofacies units and presenting them in a manner that is comparable to that used by geologists for either outcrop or core description (Ye & Rabiller, 2005).

In the Paraná Basin (see Fig. 1a), the Itararé Group includes Permo-Carboniferous stratigraphic intervals of sandstone, which are considered analogues of hydrocarbon reservoirs (França & Potter, 1988; Bocardi et al., 2006, Buso et al., 2019). The geophysical and geological data conceded by the “*Agência Nacional do Petróleo, Gás Natural e Biocombustíveis*” (ANP) of wells 1GO-1-SC and 1RCH-1-SC in western Santa Catarina state (see Fig.1b) were used to determine petrophysical parameters, such as volume shale (V_{sh}) and effective porosity (Φ_e) for the intervals corresponding to Itararé Group. These parameters were obtained using different methods, so that the effective porosity results were then evaluated for each well and used as one of the input parameters to generate electrofacies models applying the Multi-Resolution Graph-Based Clustering (MRGC) method (Ye & Rabiller, 2000). MRGC method is a multi-dimensional dot-pattern recognition method that distinguishes natural data groups, based on non-parametric k-nearest neighbors and graph data representation, not requiring priori knowledge of the data set (Ye & Rabiller, 2000). This method was applied in order to combine the effective porosity results (Φ_e), neutron porosity (NPHI), gamma ray (GR), and bulk-density (RHOB), in distinct arrangements within the lithological data, resulting into four electrofacies models. This paper aims to determine the petrophysical parameters of V_{sh} and Φ_e for the intervals corresponding to Itararé Group in the mentioned wells, and to propose electrofacies models based on different types of porosity, allowing methodological comparatives and analysis of possible relationships to the lithological intervals of the wells.

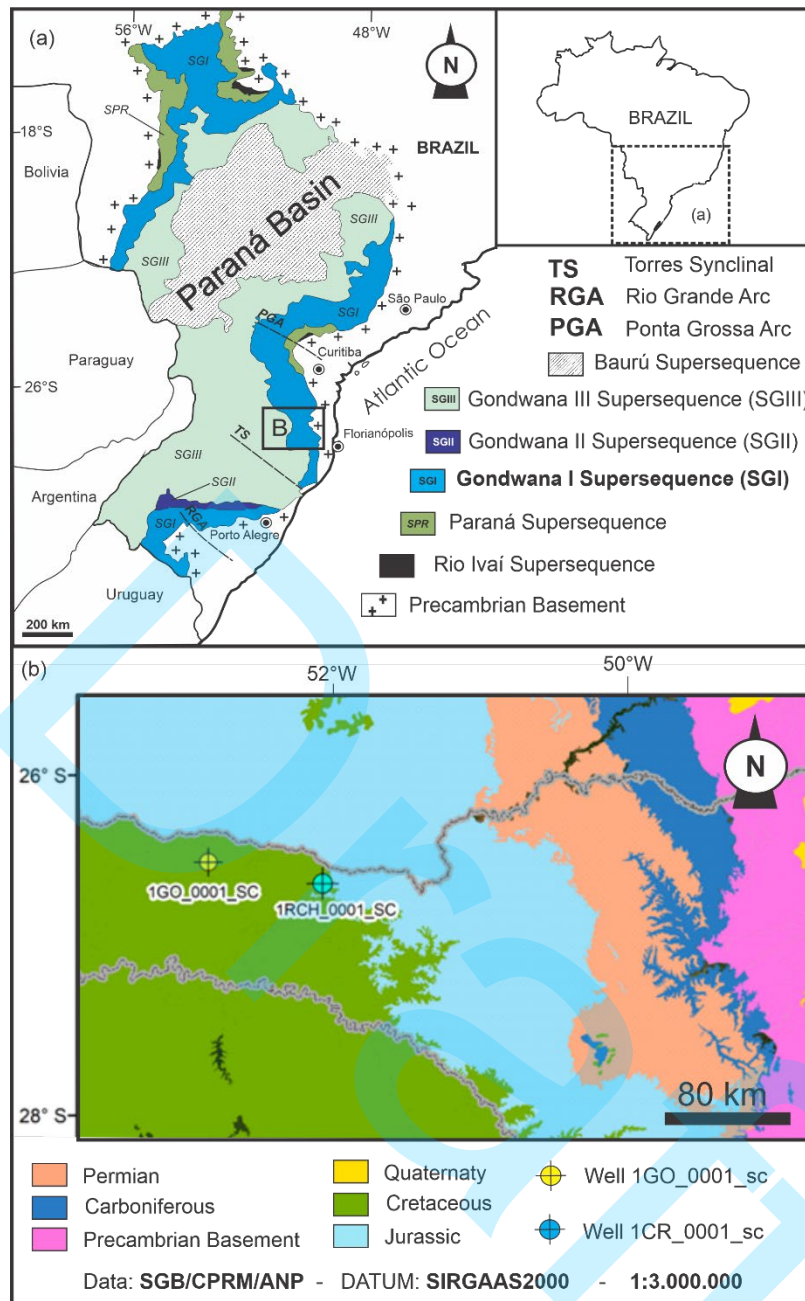


Figure 1 – (a) Simplified geologic map of the Paraná Basin with the stratigraphic Supersequences (after Milani et al., 1994); and (b) Geological map (from SGB) with locations of wells 1GO-1-SC and 1RCH-1-SC (from ANP) in western Santa Catarina state.

GEOLOGICAL CONTEXT

The Paraná Basin (Almeida et al., 1977) comprises a wide sedimentary area of approximately 1,500,000 km² whose geological history is related to cycles of tectonic subsidence and uplift that gave rise to six Supersequences limited at the top and base by unconformities (Milani et al., 2007; see Fig. 1a): Rio Ivai (Ordovician-Silurian), Paraná

(Devonian), Gondwana I (Carboniferous-Eotriassic), Gondwana II (Meso-Neo-Triassic), Gondwana III (Neo-Jurassic-Eocretaceous) and Bauru (Neo-Cretaceous).

The tectono-stratigraphic evolution of the Paraná Basin is related to the development of collisional Precambrian continental crust on the southwestern margin of the Gondwana Supercontinent, which consists of several cratonic nuclei bounded by orogenic belts composed of thrustsedimentary rocks intruded by granites (Eyles et al., 1993; see Fig. 2a).

The Itararé Group is approximately 1300 m thick and comprises the Lagoa Azul, Campo Mourão and Taciba formations (França, 1987; França & Potter, 1991; Milani, 2004; see Fig. 2b). As a result of the Serra Geral Group volcanic rocks cover, only 5 % by area of the Paraná Basin sedimentary fill is exposed (see Fig. 1a). According to Eyles et al. (1993), the oldest Itararé sedimentary succession records a glacio-lacustrine setting, though, it is possible to identify an increasing marine influence upwards through Itararé Group. The fully marine conditions are recorded by the overlying deltaic successions on top of this Group. Based on core examinations of 107 wells across the basin, Eyles et al. (1993) estimated a total logged section of over 1700 m within the Itararé Group, which comprises diamictite, conglomerate, sandstone, and siltite and shale.

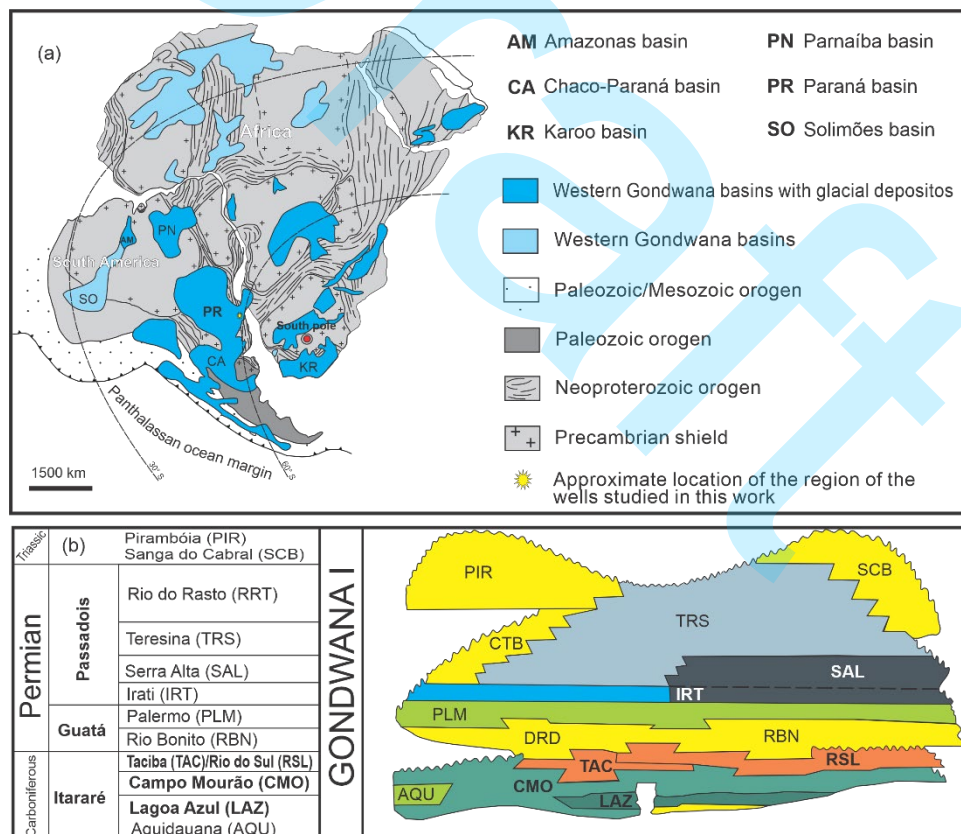


Figure 2 – (a) Geological reconstruction of West Gondwana (adapted from Malone et al., 2008; Meert et al., 2010), and (b) Stratigraphic chart of the Gondwana I Supersequence (from Milani, 2004).

METHODS

The determination of petrophysical parameters and the electrofacies modeling for the Itararé Group intervals were conducted utilizing well data provided by ANP to the project titled “*Técnicas Machine Learning para Reconhecimento de Padrões Sedimentológicos de Sistemas Turbidíticos - MLTurb*”. The methodological approach encompasses four key steps:

(i) The database structuring consisted of the integration of DLIS well files into *Geolog software*, followed by data evaluation and systematic arrangement, in layouts, of the geophysical logs in conjunction with lithological data for each well. The logs utilized in this step were: gamma ray (GR), bulk-density (RHOB) and neutron porosity (NPHI), standardized in API units, kg/m³ and V/V, respectively. The lithological data, available in AGP files (General Data Archive) was tabulated in CSV format to allow the generation of lithology intervals for each well into *Geolog software*. The layouts, which reunite GR, RHOB, and NPHI logs in conjunction with the lithological intervals, were generated to assist the determination of petrophysical parameters, and the electrofacies modeling steps.

(ii) Volume shale (V_{sh}) was determined using the gamma ray index (IGR) (Asquith & Gibson, 1982), expressed as:

$$IGR = \frac{(GR - GR_{min})}{(GR_{max} - GR_{min})} \quad (1)$$

where GR is the gamma ray reading of the formation (in API), GR_{min} represents the minimum gamma ray reading in the formation (usually found in the cleanest sandstone or limestone layers), and GR_{max} which represents the maximum gamma ray reading in the formation (typically found in the purest shale layers). The gamma ray index was also used to determine Volume shale (V_{sh}) using the Larionov method (Larionov, 1969), expressed as:

$$Vsh_{Lar} = 0.33 \cdot (2^{2 \cdot IGR} - 1), \quad (2)$$

The IGR and Larionov method results were compared for all lithological intervals, in order to evaluate the discrepancy (D) between these methods, expressed as:

$$D = | \underline{IGR} - \underline{Vsh}_{Lar} |, \quad (3)$$

where \underline{IGR} is the mean V_{sh} value for a given lithological interval, obtained by the gamma ray

index, while Vsh_{Lar} is the mean V_{sh} value for a given lithological interval, obtained by the Larionov method.

(iii) Effective porosity (Φ_e) was determined using the density method (Φ_{eD}) (Asquith & Gibson, 1982) and the neutron-density method (Φ_{eND}) (Bateman & Konen, 1977). The effective porosity from the density method is basically obtained from the density-porosity formula, adjusted to the effect caused by the presence of shales in a formation's total porosity, as expressed in the following equation:

$$\Phi_{eD} = \frac{(\rho_m - \rho_b)}{(\rho_m - \rho_f)} - Vsh \cdot \frac{(\rho_m - \rho_{sh})}{(\rho_m - \rho_f)}, \quad (4)$$

where ρ_m is the rock matrix density, or, the formation's solid framework density (in kg/m^3), ρ_b represents the bulk-density readings from RHOB log (in kg/m^3), ρ_f corresponds to the density of the fluid existing in the formation (in kg/m^3), ρ_{sh} corresponds to the representative density value for shales (kg/m^3), and V_{sh} (V/V) represents the volume shale of the formation. The effective porosity using the neutron-density method (Φ_{eND}) consists of a crossplot of the results obtained from Eq. 4 with the results of effective porosity obtained from the neutron porosity log (NPHI), the last being determined by the following expression:

$$\Phi_{eN} = \Phi_N - Vsh \cdot \Phi_{Nsh}, \quad (5)$$

where Φ_N corresponds to the neutron porosity readings from the NPHI log (in V/V), Φ_{Nsh} is the representative neutron porosity value for shales (in V/V), and V_{sh} corresponds to the volume shale of the formation (in V/V). The neutron-density method (Φ_{eND}) calculation is automatically executed by *Geolog Software* (Emerson), as long the analyst provides all required input data. All logs and constants required to calculate Φ_e (using both methods) were available in the well files. The V_{sh} results utilized for the calculation of both Φ_{eD} and Φ_{eND} were those obtained from Eq. 2, since the Itararé Group comprises rocks older than Tertiary (Larionov, 1969). The effective porosity results (Φ_{eD} and Φ_{eND}) were also compared for all lithological intervals, to evaluate the discrepancy (E) between these methods, expressed as:

$$E = | \underline{\Phi_{eND}} - \underline{\Phi_{eD}} |, \quad (6)$$

where $\underline{\Phi_{eND}}$ is the mean effective porosity value for a given lithological interval, obtained by the neutron-density method, while $\underline{\Phi_{eD}}$ is the mean effective porosity value for a given lithological

interval, obtained by the density method.

(iv) The electrofacies models were created using the Multi-Resolution Graph-Based Clustering (MRGC) method. Log data input included: GR, RHOB, NPFI, Φ_{eD} , and Φ_{eND} . The lithological intervals were inserted as “associated logs”, functioning as a validation basis for the resulting models. In this manner, the software can relate the clusters’ samples (elements) to each one of the lithological intervals in the modeling process. The Euclidian metric was adopted in this work, as well as an initial number of 4 neurons in the Coarse-to-fine Self-Organizing Map (CFSOM). The MRGC method automatically provides an optimal number of clusters, though the user is allowed to manage the level of detail needed to characterize the electrofacies (Ye & Rabiller, 2000). It was set to a minimum of 8 and a maximum of 12 initial clusters in the MRGC modeling process to attain a pattern of 8 final electrofacies for each model. In cases where the number of clusters was greater than 8, those with closer values of GR , $RHOB$, and similar samples contingency were merged to satisfy the 8-electrofacies pattern. For each well, two types of models were created, each based on a different porosity log input in addition to the other geophysical logs (see Table 1).

Table 1 – Model Identification, quantity of samples, number of initial clusters defined by Geolog Software, and logs used to generate the electrofacies models. (LITH = lithology log; GR = gamma ray log; RHOB = bulk-density log, and Φ = porosity log).

Well	Model ID	Samples	Clusters	Logs			
				LITH	GR	RHOB	Φ
1GO-1-SC	GO1	3246	10	<input type="checkbox"/>	<input type="checkbox"/>	<input type="checkbox"/>	NPFI
	GO2	3245	12	<input type="checkbox"/>	<input type="checkbox"/>	<input type="checkbox"/>	Φ_{eD}
1RCH-1-SC	RC1	4758	9	<input type="checkbox"/>	<input type="checkbox"/>	<input type="checkbox"/>	NPFI
	RC2	4758	10	<input type="checkbox"/>	<input type="checkbox"/>	<input type="checkbox"/>	Φ_{eND}

RESULTS AND DISCUSSIONS

Database Structuring

The lithological intervals for each well (from AGP files) allowed us to determine and quantitatively analyze the total thicknesses of each unit in the wells, as can be seen in Figure 3a. Thus, it was possible to observe that the lithologies corresponding to diamictite represent the main intervals in both wells. The sandstone and siltstone intervals in both wells have very similar thicknesses, on the other hand, the intervals corresponding to shales are considerably different in both wells. Only in well 1GO-1-SC does a relatively thin interval of calcilitite (~2 m) occur, and for this reason it was not considered in the calculations to determine the petrophysical

parameters of this well.

Two lithostratigraphic profiles were prepared from the lithological data of each well (see Fig. 3b). In these profiles it was possible to observe two patterns of strata succession: retrogradational and progradational. The lower portions of these two wells mainly comprise thinning upward cycles of the diamictite, followed by thickening upward cycles. This is an evident decrease and increase in energy and sediment input, respectively. On the other hand, only in the upper portion of the 1RCH-1-SC well profile does a retrogradational succession occur with a dominance of sandstones at the base that are followed by shales (rhythmites?) at the top. This is a characteristic pattern of unconfined and confined (channeled) distal turbidite systems of the Taciba Formation. The basal portion of this succession is marked by a (probable) transgressive stratigraphic surface, which explains the increase in shale content in these strata.

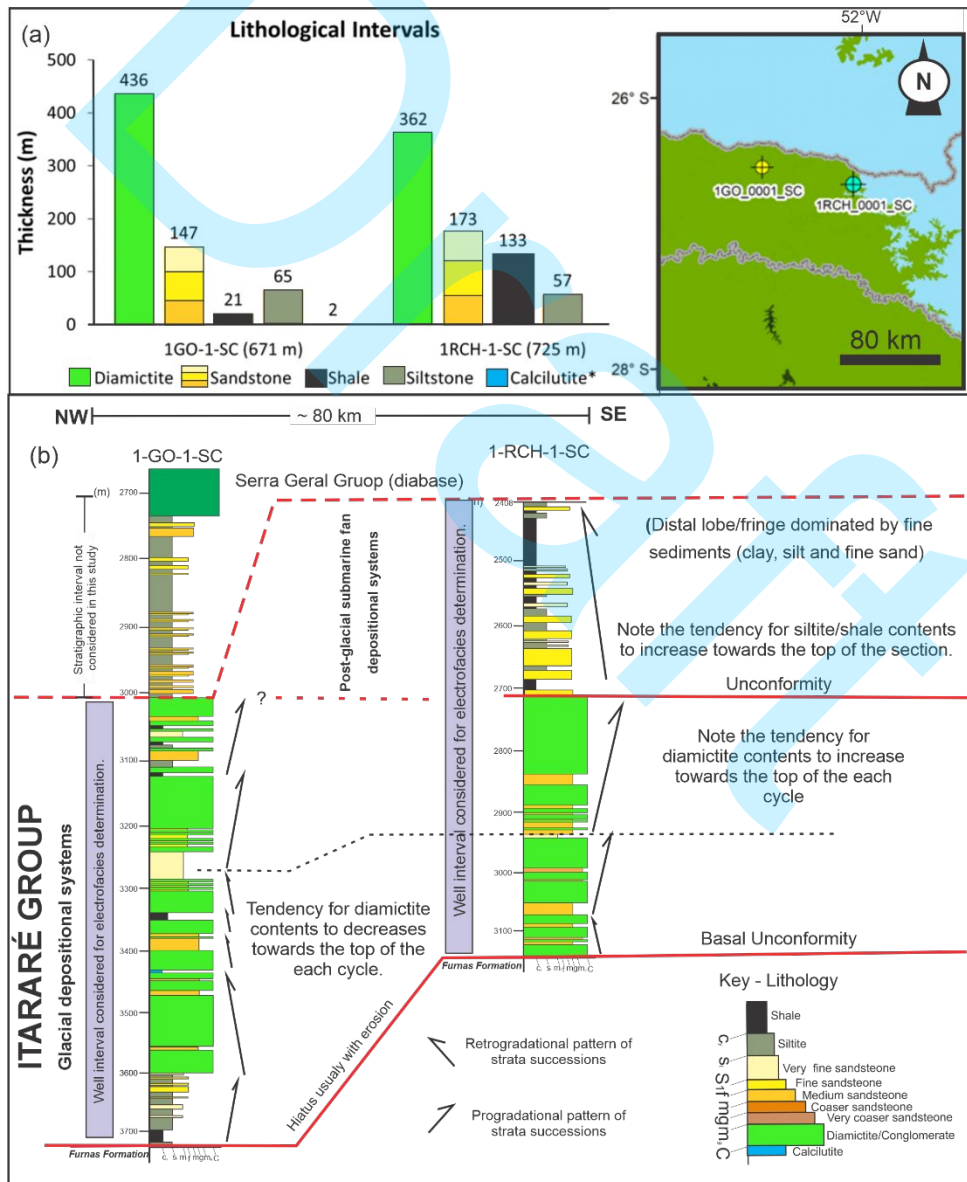


Figure 3 – (a) Lithological intervals in wells 1GO-1-SC and 1RCH-1-SC: the lithological intervals represent the sum of all beds thicknesses of a given lithological unit. 671 m and 725 m are the sum of all interval's thicknesses in each well. *Disregarded lithological interval; and (b) Lithostratigraphic profiles prepared

from lithological data from each well.

Volume shale (V_{sh})

The results present differences according to the method used for the calculation of V_{sh} , as well as differences related to the lithological types of the wells. Table 2 exhibits minimums, maximums and means values (IGR and Vsh_{Lar}) of V_{sh} (V/V), obtained by IGR and Larionov methods for each lithological intervals of the wells.

The Larionov method determined the absolute maximum V_{sh} value of 0.990 V/V for the shale interval, and the absolute minimum V_{sh} value of zero for the sandstone interval, for both wells. The mean V_{sh} values (Vsh_{Lar}) are greater for the shale intervals and lower for the sandstone intervals. In well 1GO-1-SC V_{sh} mean values are greater than those in well 1RCH-1-SC for all intervals, except diamictite. In well 1GO-1-SC, diamictite and siltite intervals exhibit similar V_{sh} mean values.

The IGR method determined the absolute maximum V_{sh} value of 1 V/V for the shale interval, and the absolute minimum V_{sh} value of zero for the sandstone interval, for both wells. The mean V_{sh} values (IGR) are greater for the shale intervals and lower for the sandstone intervals. In well 1GO-1-SC V_{sh} mean values using the IGR method are greater than those in well 1RCH-1-SC for all intervals, except diamictite.

Comparing the V_{sh} results (minimums, maximums and means) of each method, it is noticeable that the IGR method returns higher values than those determined by Larionov's method. This effect is also noticed in the histograms of Vsh_{Lar} and IGR for the complete lithological interval of the wells (see Fig. 4). In wells 1GO-1-SC and 1RCH-1-SC, the discrepancy between results (D) has its lowest values in the sandstone intervals, followed by shale, siltite and diamictite intervals. Conducting the equivalence comparison between intervals in the wells, it was possible to observe that the D values are similar. In general, and considering that only 1RCH-1-SC has the upper portion that is richer in shale (post-glacial distal turbidites), it is observed that the D values are very similar.

Table 2 – V_{sh} values (V/V) for wells 1GO-1-SC and 1RCH-1-SC. Vsh_{Lar} and IGR are the mean Vsh values for each lithological interval of the wells. The “Total” represents Vsh values for the complete studied stratigraphic intervals.

Well	Interval	Vsh_{Lar}			IGR			D
		<i>min.</i>	<i>max.</i>	Vsh_{Lar}	<i>min.</i>	<i>max.</i>	IGR	
1GO-1-SC	Diamictite	0.074	0.706	0.338	0.146	0.825	0.500	0.162
	Sandstone	0	0.487	0.141	0	0.654	0.246	0.105

	Shale	0.306	0.990	0.631	0.474	1	0.760	0.129
	Siltistone	0.033	0.839	0.329	0.069	0.912	0.473	0.144
	Total	0	0.990	0.303	0	1	0.449	0.146
1RCH-1-SC	Diamictite	0.079	0.649	0.343	0.156	0.784	0.508	0.165
	Sandstone	0	0.479	0.133	0	0.646	0.236	0.103
	Shale	0.061	0.990	0.477	0.123	1	0.623	0.146
	Siltistone	0.092	0.650	0.291	0.178	0.785	0.448	0.157
	Total	0	0.990	0.314	0	1	0.459	0.145

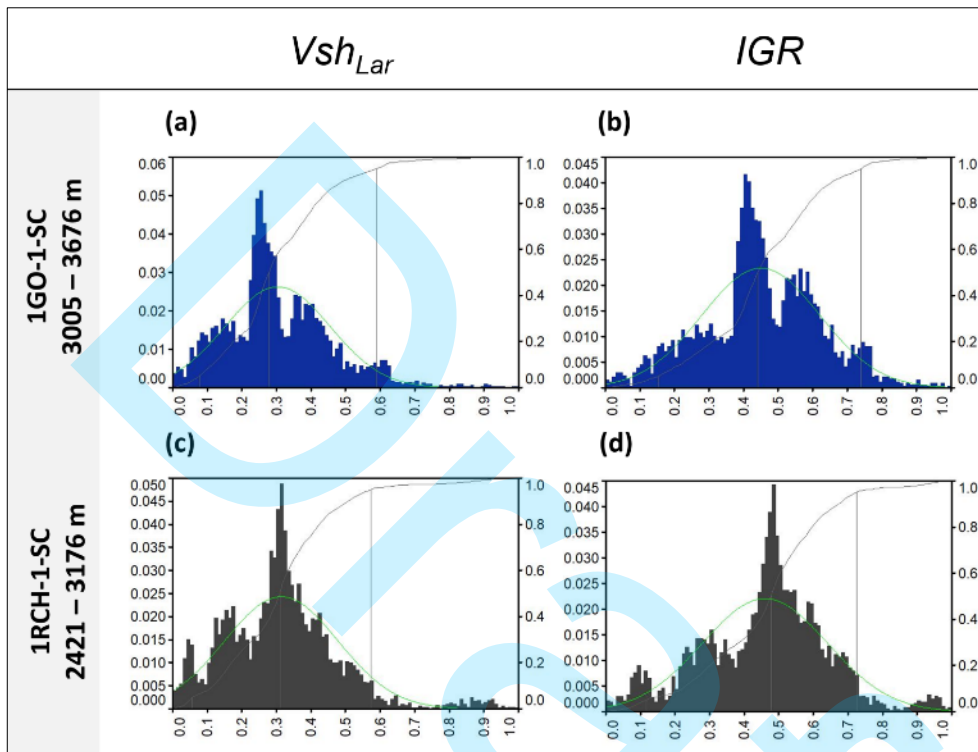


Figure 4 – Comparative histograms of V_{sh} values determined by Larionov method ($V_{sh_{Lar}}$) and gamma ray index (IGR) for wells 1GO-1-SC (a and b); and 1RCH-1-SC (c and d). Y axis (left side): frequency (fraction). Y axis (right side): accumulated fraction of data. X axis: volume shale (V/V). The depths are relative to the interval corresponding to Itararé Group in the wells.

Effective Porosity (Φ_e)

The effective porosity results present differences according to the method used for its determination, which are noticeable in terms of the lithological intervals of the wells. Table 3 exhibits minimums, maximums and means values (Φ_{eD} and Φ_{eND}) of effective porosity (V/V), for each of the lithological intervals of the wells.

In 1GO-1-SC well, the values of Φ_{eD} are similar or slightly lower than the values of Φ_{eND} for each interval, so that the discrepancy of these means (E) is lower for the sandstone and siltite intervals (0.003 and 0.003, respectively), followed by diamictite and shale intervals (0.017 and 0.029, respectively). In this well, Φ_{eD} and Φ_{eND} present similar values for the sandstone interval, 0.080 and 0.077, respectively (see Fig. 5).

In well 1RCH-1-SC, the Φ_{eD} maximum values are remarkably higher than the Φ_{eND} maximum values. This pattern extends for the mean porosity values ($\underline{\Phi_{eD}}$ and $\underline{\Phi_{eND}}$) of each interval, so that the discrepancy of these means (E) is lower for the shale interval (0.027), followed by diamictite (0.049), siltite (0.053) and sandstone (0.085) intervals. In this well, the $\underline{\Phi_{eD}}$ is 0.191 and the $\underline{\Phi_{eND}}$ is 0.106 for the sandstone intervals (see Fig. 5).

According to França & Potter (1989), the porosity of the Itararé Group sandstones is intergranular type and secondary, representing approximately 10% of rock volume. For 1GO-1-SC well, $\underline{\Phi_{eD}}$ and $\underline{\Phi_{eND}}$ values for the sandstone interval corroborate the estimate given by these authors, while for 1RCH-1-SC well, only $\underline{\Phi_{eND}}$ values corroborate this estimate.

Table 3 – Effective porosity (Φ_{eD} and Φ_{eND}) for wells 1GO-1-SC and 1RCH-1-SC. $\underline{\Phi_{eD}}$ and $\underline{\Phi_{eND}}$ represent the mean values for each lithological interval of the wells.

Well	Interval	Φ_{eD}			Φ_{eND}			E
		<i>min.</i>	<i>max.</i>	$\underline{\Phi_{eD}}$	<i>min.</i>	<i>max.</i>	$\underline{\Phi_{eND}}$	
1GO-1-SC	Diamictite	0	0.223	0.058	0.025	0.198	0.075	0.017
	Sandstone	0	0.258	0.080	0.018	0.229	0.077	0.003
	Shale	0	0.128	0.030	0	0.122	0.059	0.029
	Siltistone	0.007	0.230	0.075	0.020	0.214	0.078	0.003
	Total	0	0.258	0.063	0	0.229	0.075	0.012
1RCH-1-SC	Diamictite	0.069	0.199	0.118	0.016	0.122	0.069	0.049
	Sandstone	0	0.268	0.191	0.004	0.174	0.106	0.085
	Shale	0	0.239	0.111	0	0.198	0.084	0.027
	Siltistone	0.096	0.219	0.159	0.041	0.183	0.106	0.053
	Total	0	0.268	0.138	0	0.198	0.083	0.055

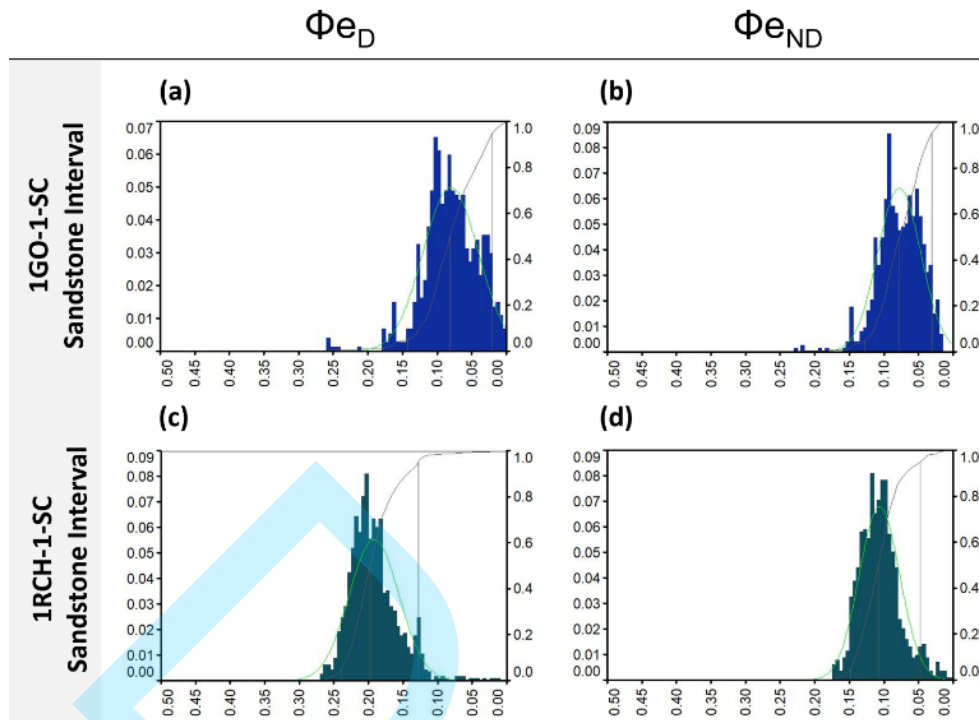


Figure 5 – Comparative histograms of effective porosity values determined by the density method (Φ_{eD}) and neutron-density method (Φ_{eND}) for the sandstone interval of wells 1GO-1-SC (a and b) and 1RCH-1-SC (c and d). Y axis (left side): frequency (fraction). Y axis (right side): accumulated fraction of data. X axis: effective porosity (V/V).

Electrofacies Models

Two electrofacies models were defined for each well: GO1 and GO2 (1GO-1-SC well); and RC1 and RC2 (1RCH-1-SC well). These models were represented in layout along with the lithological data and the geophysical curves used for the MRGC modeling process. The electrofacies were analyzed in relation to the lithologies of the wells, allowing the delimitation of electrofacies associations (see Figs. 6 and 7).











The samples contingency for all electrofacies models (after merging similar clusters) is shown in the Table 4, where it is possible to verify the contribution of each lithological interval to the number of samples assigned to the models' electrofacies, as well as its equivalent in percentage. The samples contingency was used as a reference to evaluate the representativeness of the electrofacies for the studied lithological intervals in the wells.

Table 5 groups representative data of the electrofacies determined for GO1, GO2, RC1 and RC2 models. The table exhibits mean values for GR, RHOB, and mean porosity values (NPHI, Φ_{eD} or Φ_{eND}) for each electrofacies of the models. The weights refer to the total number of samples associated to each one of the electrofacies (see Tables 4 and 5). The visual representation of the electrofacies in the model layouts (see Figs. 6 and 7) was given according to the colors displayed in Table 5.

Table 4 – Contingencies (samples count): number of samples assigned to the electrofacies of GO1, GO2, RC1 and RC2 models as a function of the lithological intervals of the Itararé Group. The percentual values are relative to the total of samples in each electrofacies. The electrofacies total number of samples represent its weight in the model. *DM* = diamictite; *SS* = sandstone; *SH* = shale and *ST* = siltite.

Contingencies (samples count)									
ID	Interval	A1	A2	A3	A4	A5	A6	A8	A9
GO1	DM	335 (70%)	161 (71%)	659 (90%)	717 (78%)	172 (60%)	25 (14%)	15 (5%)	1 (1%)
	SS	4 (1%)	5 (2%)	45 (6%)	88 (10%)	85 (30%)	135 (77%)	238 (82%)	140 (99%)
	SH	84 (18%)	10 (4%)	8 (1%)	-	-	-	-	-
	ST	55 (12%)	52 (23%)	21 (3%)	110 (12%)	28 (10%)	15 (9%)	38 (13%)	-
	Total	478	228	733	915	285	175	291	141
		A1	A2	A3	A4	A5	A6	A7	A10
GO2	DM	244 (67%)	191 (68%)	450 (90%)	1000 (84%)	138 (67%)	55 (18%)	6 (2%)	1 (1%)
	SS	5 (1%)	3 (1%)	23 (5%)	103 (9%)	40 (19%)	198 (65%)	254 (95%)	110 (84%)
	SH	76 (21%)	20 (7%)	7 (1%)	2 (0%)	-	-	-	-
	ST	40 (11%)	65 (23%)	20 (4%)	87 (7%)	29 (14%)	50 (17%)	8 (3%)	20 (15%)
	Total	365	279	500	1192	207	303	268	131
		B1	B2	B3	B4	B6	B7	B8	B9
RC1	DM	-	65 (22%)	964 (65%)	388 (96%)	843 (73%)	93 (45%)	21 (2%)	-
	SS	-	1 (0%)	45 (3%)	-	84 (7%)	90 (44%)	716 (83%)	199 (99%)
	SH	144 (100%)	224 (75%)	269 (18%)	10 (2%)	189 (16%)	6 (3%)	29 (3%)	3 (1%)
	ST	-	7 (2%)	210 (14%)	5 (1%)	36 (3%)	16 (8%)	100 (12%)	1 (0%)
	Total	144	297	1488	403	1152	205	866	203
		B1	B2	B3	B5	B6	B7	B8	B9
RC2	DM	-	52 (19%)	651 (69%)	578 (65%)	973 (76%)	21 (66%)	99 (11%)	-
	SS	-	-	18 (2%)	53 (6%)	81 (6%)	10 (31%)	691 (74%)	282 (99%)
	SH	123 (100%)	221 (80%)	189 (20%)	121 (14%)	190 (15%)	-	28 (3%)	2 (1%)
	ST	-	2 (1%)	84 (9%)	139 (16%)	38 (3%)	1 (3%)	111 (12%)	-
	Total	123	275	942	891	1282	32	929	284

Table 5 – Identification, colors (hexadecimal code), weights and mean values of GR, RHOB and porosity (NPHI, Φ_{eD} or Φ_{eND}) of the electrofacies determined for GO1, GO2, RC1 and RC2 models.

1GO-1-SC							
Model	ID	Color		Weight	\overline{GR} (API)	\overline{RHOB} (kg/m ³)	Porosity (V/V)
		Swatch	Hex Code				\overline{NPHI}
GO1	A1		#3533cc	478	110.23	2629.04	0.115
	A2		#a020f0	228	108.55	2232.23	0.190
	A3		#adff2f	733	88.55	2643.11	0.070
	A4		#da70d6	915	74.04	2603.14	0.056
	A5		#ffc0cb	285	71.99	2437.65	0.090
	A6		#d60005	175	58.35	2526.75	0.060
	A8		#ffaa00	291	42.60	2577.50	0.030
	A9		#ffd600	141	42.09	2473.28	0.070
							Φ_{eD}
GO2	A1		#3533cc	365	112.00	2643.58	0.020
	A2		#a020f0	279	109.35	2275.82	0.139

	A3		#adff2f	500	93.86	2641.98	0.022
	A4		#da70d6	119 2	76.82	2607.93	0.046
	A5		#ffc0cb	207	69.63	2406.77	0.160
	A6		#d60005	303	56.01	2568.01	0.060
	A7		#ff6300	268	50.88	2496.35	0.110
	A10		#ffff96	131	33.70	2610.27	0.040
1RCH-1-SC							
<i>NPHI</i>							
RC1	B1		#006400	144	84.36	2665.48	0.210
	B2		#3533cc	297	67.69	2624.54	0.150
	B3		#a020f0	148 8	57.40	2602.61	0.120
	B4		#adff2f	403	54.66	2655.11	0.082
	B6		#da70d6	115 2	47.45	2633.85	0.050
	B7		#ff6300	205	37.77	2570.09	0.070
	B8		#ffd600	866	34.50	2501.43	0.110
	B9		#ffff96	203	20.44	2540.42	0.080
	<i>ϕe_{ND}</i>						
RC2	B1		#006400	123	85.80	2670.72	0.040
	B2		#3533cc	275	68.60	2616.86	0.110
	B3		#a020f0	942	61.00	2621.91	0.091
	B5		#9370db	891	53.28	2595.12	0.090
	B6		#da70d6	128 2	48.00	2638.83	0.050
	B7		#ff6300	32	38.10	2566.28	0.080
	B8		#ffd600	929	35.58	2514.42	0.110
	B9		#ffff96	284	20.95	2527.41	0.100

Electrofacies of the GO1 and GO2 models

The A1 electrofacies presents the highest *GR* and *RHOB* values among other electrofacies. The neutron porosity (*NPHI*) for this electrofacies is higher than the effective porosity (*ϕe_D*), which is probably associated to a higher shale content. The electrofacies is related to diamictite, shales and siltstones, comprising approximately 70%, 20% and 10% of the samples attributed to the electrofacies, respectively. This electrofacies is mainly recorded from 3020 to 3210 m, and subordinately, from 3340 to 3375 m. In these intervals, A1 electrofacies is usually in association with A2 and A3 electrofacies.

The A2 electrofacies has immediately lower *GR* values than those of the A1 electrofacies. However, A2 electrofacies has the lowest *RHOB* values as well as the highest *NPHI* and *ϕe_D* values among other electrofacies. The A2 electrofacies is related to diamictite, siltstones and

shales, which comprise about 70%, 23% and 5% of the samples attributed to the electrofacies, respectively. The A2 electrofacies was mainly recorded from 3050 to 3200 m in depth. In this interval, A2 electrofacies is in association with A1 electrofacies. There are minor records of A2 electrofacies below 3665 m in depth, which are related to siltstones adjacent to sandstones. In general aspects, A2 electrofacies is an electrofacies of anomalous characteristics in relation to bulk-density and porosity values. These characteristics may reflect the drilling conditions of the well, such as wall collapses, unconsolidated materials, and instrumental errors during data collection, among others. The analysis of the caliper log may help in a better understanding of these conditions.

The A3 electrofacies has GR values close to 90 API, $RHOB$ values of approximately 2640 kg/m³, and is related to diamictite and sandstones, comprising 90% and 6% of the samples attributed to the electrofacies, respectively. This electrofacies is recorded mainly from 3005 to 3375 m in depth, mostly where diamictite are next to shales or, next to sandstones. In the first case, A3 electrofacies is in association with A1 electrofacies, and in the second it is in association with A4 electrofacies. In GO1 model, there are also records of A3 electrofacies below 3375 m in depth, related to diamictite adjacent to sandstones. In this case, A3 electrofacies is in association with A4 electrofacies. The A3 electrofacies associations with other electrofacies suggest that there are areas of relatively gradual transition between diamictite and shales sections and, between diamictite and sandstones sections. The A3 electrofacies has second highest weight in both models.

The A4 electrofacies present GR and $RHOB$ values close to 75 API and 2605 kg/m³, respectively, and have the highest weight in GO1 and GO2 models. The mean porosity values ($NPHI$ and ϕ_{eD}) are similar and relatively low (~ 0.05 V/V). In GO1 model, A4 electrofacies is related to diamictite (78%), siltstones (12%) and sandstones (10%). In GO1 model, A4 electrofacies is mainly recorded from 3305 to 3676 m in depth, being primarily in association with A3 electrofacies and secondarily to A6, A8 or A5 electrofacies. In GO2 model, the proportion of samples is approximately 84% (diamictite), 8% (siltstones) and 8% (sandstones). In GO2 model, A4 electrofacies is recorded from 3005 to 3360 m, being usually in association with A3 electrofacies in diamictite sections, and to A6 and A7 electrofacies where diamictite intercalate with sandstones. From 3400 to 3653 m in depth A4 electrofacies is usually recorded in association with electrofacies A5, A6 or A10, in diamictite or siltstone sections. In general aspects, the records of A4 electrofacies are more homogeneous in both models, which is possibly a reflection of the electrofacies weight, being the highest among other electrofacies.

The A5 electrofacies has GR (71 API) and $RHOB$ (2420 kg/m³) values and is related to diamictite (63%), sandstones (25%) and siltite (12%). In GO1 model, this electrofacies was recorded below 3247 m in depth, where it is usually in association with A4 electrofacies in

diamictite sections, and to A4 and A6 electrofacies in sandstones or siltstones sections. In GO2 model, the A5 electrofacies was registered below 3055 m, exhibiting less records than observed in GO1 model. In this case, this electrofacies is usually in association with A4 electrofacies in diamictite sections, and to A4 and A7 electrofacies in sandstone or siltstone sections. In general aspects, A5 electrofacies presents few records within the models, although, its relationship to other electrofacies suggests that there are zones of a relatively gradual transition between diamictites and sandstones.

The A6 electrofacies has \underline{GR} (57 API) and \underline{RHOB} (2550 kg/m³) values, and presents low porosity values. In GO1 model, A6 electrofacies is related to sandstones (77%), siltstones (19%), and diamictite (14%). In GO1 model, A6 electrofacies is recorded from 3212 to 3475 m in depth, in intervals of sandstones that are next or intercalated with diamictite, and below 3630 m in depth, in siltstone sections. In these intervals, A6 electrofacies is in association with A4, A5, A8 and A9 electrofacies. For GO2 model, the proportion of samples is 65% (sandstone), 18% (diamictite) and 17% (siltstone). In GO2 model, A6 electrofacies was recorded on almost the same intervals mentioned for GO1 model, although varying its distribution within the sections of occurrence and the electrofacies it associates with. In this case, the A6 electrofacies is usually in association with A4 and A7 electrofacies from 3212 and 3475 m in depth, and to A4 and A10 electrofacies below 3610m in depth.

The A7 electrofacies occurs only in GO2 model, presenting \underline{GR} (51 API) and \underline{RHOB} (2496 kg/m³) values, and $\underline{\Phi e_D}$ value of 0.1 V/V. This electrofacies is almost entirely related to sandstones, comprising about 95% of the samples assigned to the electrofacies. In this model, the records of A7 electrofacies are mainly related to sections of sandstone next to diamictites in the range from 3217 to 3475 m in depth, where it commonly associates with A6 and/or A4 electrofacies.

The A8 electrofacies, was defined only in GO1 model, presents \underline{GR} (42 API) and \underline{RHOB} (2575 kg/m³) values, a low \underline{NPFI} value (~0.03 V/V), and is related to sandstones (83%), siltstones (12%) and diamictite (5%). In this model, this electrofacies is recorded below 3375 m in depth, mainly in sandstone intervals that are next to diamictite or intercalated with siltstones. There are only minor records above this range. Additionally, this electrofacies is usually in association with electrofacies A4, A6, A9 or A5 for the mentioned depth.

The A9 electrofacies (defined only in GO1 model) presents a \underline{GR} value like that of the previous electrofacies. Nevertheless, \underline{RHOB} value is lower and \underline{NPFI} value is higher than that of A8 electrofacies. This electrofacies is related to sandstones, comprising 99% of the samples assigned to the electrofacies, being recorded mainly from 3055 to 3475 m in depth. In this interval, A9 electrofacies is commonly seen in association with A6 and A8 electrofacies.

The A10 electrofacies occurs only in model GO2 and has a \underline{GR} value of 34 API, being the lowest among other electrofacies. This electrofacies presents \underline{RHOB} (2610 kg/m³) and $\underline{\Phi e_D}$ (0.04

V/V) values and is related to sandstones (84%) and siltstones (15%) of the samples assigned to the facies. In this model, A10 electrofacies is recorded from 3560 to 3676 m in depth, in sandstone intervals that are adjacent to siltstones, being commonly seen in association with A6 and/or A4 electrofacies.

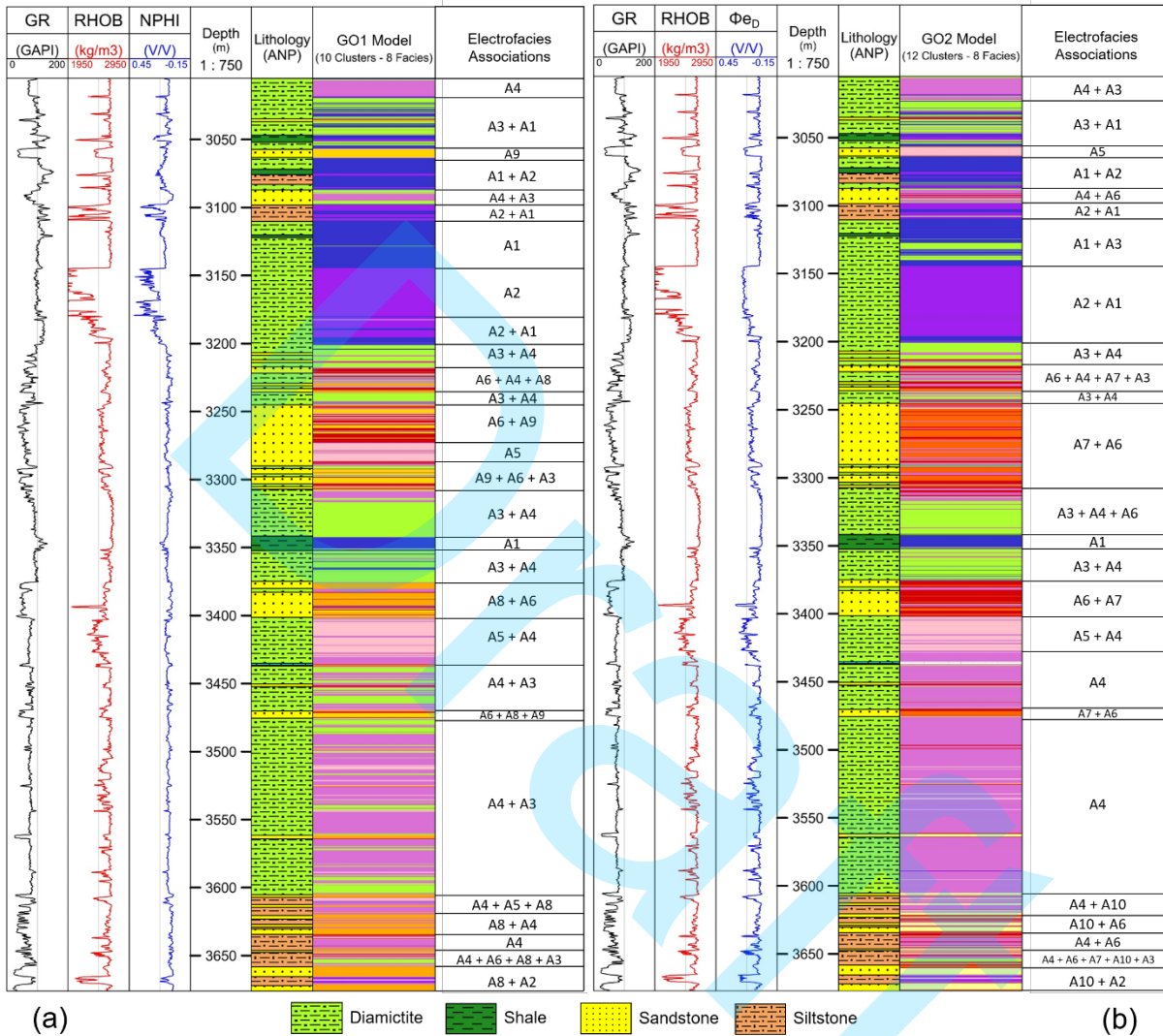


Figure 6 – Models determined for 1GO-1-SC well based on the neutron porosity log (a), and effective porosity determined by the density method (b)

The GO1 and GO2 models comprise electrofacies in which the elements assigned to the diamictite interval predominate, followed by the sandstones interval. The shales interval represents only 3% of the total rock stacking of Itararé Group in this well, reflecting in low numbers of samples and low representativeness within the models. Similarly, siltstones exhibit low representativeness within the models, corresponding to less than 10% of the total rock stacking of the well.

Electrofacies of the RC1 and RC2 models

The B1 electrofacies presents the highest GR (85 API) and $RHOB$ (2670 kg/m³) values among other electrofacies. The neutron porosity mean value ($NPHI$) for the electrofacies is much higher than the effective porosity (ϕ_{eND}), which is most likely related to the shale content of the samples, since B1 electrofacies is exclusively related to shales (100% of the samples). In both models, B1 electrofacies is mainly recorded from 2535 to 2942 m, presenting only a minor record above this range, which is in association with B2 electrofacies.

The B2 electrofacies presents GR values close to 68 API and $RHOB$ values slightly lower than that in electrofacies B1. The $NPHI$ value is higher than ϕ_{eND} , although the difference is less pronounced than that observed in electrofacies B1. The B2 electrofacies is related to shales (78%) and diamictite (21%), and in RC1 model, is recorded in shale sections from 2435 to 2700 m in depth, and in diamictite sections from 2700 to 2950 m in depth. In these intervals, B2 electrofacies is commonly seen in association with electrofacies B3. In RC2 model, B2 electrofacies is recorded in shale sections from 2435 to 2700 m in depth, and in diamictite sections from 2700 to 2832 m in depth. In these intervals, B2 electrofacies is in association with B3 and/or B5 electrofacies.

The B3 electrofacies has GR and $RHOB$ values like those of B2 electrofacies. The $NPHI$ value is relatively close to ϕ_{eND} . This electrofacies is related to diamictite (68%), shales (21%) and siltstones (8%) of the samples assigned to the electrofacies. In RC1 model, B3 electrofacies was recorded from 2421 to 2964 m in depth, where one can identify: associations with B2 and B6 electrofacies in shale sections; associations with B2, B4 and B6 electrofacies in diamictite sections; and associations with B6 and B7 electrofacies in siltstone sections. In RC2 model, B3 electrofacies was recorded in shale sections from 2421 to 2560 m in depth, where it commonly associates with B2 and B5 electrofacies; and in diamictite sections from 2710 to 2970 m in depth, where it frequently associates with B2, B5 and B6 electrofacies. Ultimately, this electrofacies presents the highest weight in RC1 model and the second highest weight in RC2 model.

The B4 Electrofacies (defined only in RC1 model) presents GR (55 API) and $RHOB$ (2655 kg/m³) values, and the $NPHI$ value is lower than those of previous electrofacies (~0.08 V/V). This electrofacies is related to diamictite (96%) and shales (2%) of the samples attributed to electrofacies. In this model, B4 electrofacies is recorded from 2770 to 2890 m in depth, where it associates with B3 and B6 electrofacies, as well as from 2960 to 3050 m in depth, where it associates with only B6 electrofacies.

The B5 electrofacies, which occurs only in RC2 model, presents GR and $RHOB$ values slightly lower than that of the B4 electrofacies, an effective porosity (ϕ_{eND}) of 0.09 V/V, and is

related to diamictite (65%), siltstones (16%) and shales (14%). The B5 electrofacies is primarily recorded in diamictite sections from 2710 to 2880 m in depth and, secondarily, in shale and siltstone sections from 2421 to 2670 m in depth. In both intervals, B5 electrofacies typically associates with B3 and B6 electrofacies, with slight affiliations with B2 electrofacies.

The B6 electrofacies presents \underline{GR} (48 API), \underline{RHOB} (2635 kg/m³), and \underline{NPHI} and $\underline{\phi_{e_{ND}}}$ coincident and low (0.05 V/V). This electrofacies is related to diamictite (75%), shales (15%) and sandstones (7%) of the samples attributed to the electrofacies. In the RC1 model, B6 electrofacies is recorded from 2475 to 2600 m in depth, where it apparently delineates zones of transition (to sandstone sections) within shale or siltstone sections. Furthermore, this electrofacies is also related to diamictite sections between 2883 and 3145 m in depth, where it commonly associates with B4 electrofacies. In the RC2 model, B6 electrofacies was registered in the same depth intervals described for RC1 model. In the first one, B6 electrofacies associates with B5 electrofacies. In the second interval, it primarily associates with B5 and B3 electrofacies and, secondarily, with B8 electrofacies. Ultimately, this electrofacies presents the highest weight in RC2 model and the second highest weight in RC1 model.

The B7 electrofacies exhibits \underline{GR} (38 API) and \underline{RHOB} (2570 kg/m³) values, and mean porosity slightly higher than those of B6 electrofacies, being $\underline{NPHI} < \underline{\phi_{e_{ND}}}$. In the RC1 model, B7 electrofacies is related to diamictite, sandstones and siltstones, comprising 45%, 44% and 8% of the samples assigned to the electrofacies, respectively, while this proportion is 66%, 31% and 3% for the same intervals of the RC2 model. The B7 electrofacies is mainly registered in intercalations of diamictite and sandstones between 2890 and 2940 m in depth, where it commonly associates with B6 and/or B8 electrofacies.

The B8 electrofacies presents \underline{GR} and \underline{RHOB} values close to 35 API and 2510 kg/m³, respectively. In the RC1 model, electrofacies B8 is related to sandstones, siltstones and diamictite, which comprise approximately 82%, 13% and 2% of the samples attributed to electrofacies, respectively. In the RC2 model, the proportion is 74%, 12% and 11%, for these intervals. When compared to other electrofacies associated with sandstones, this electrofacies has the greatest mean porosity values, in which $\underline{NPHI} = \underline{\phi_{e_{ND}}} = 0.11$ V/V. The B8 electrofacies is recorded across the Itararé Group interval in several well sections, in which it associates with B3, B5, and B6 electrofacies where sandstones and siltstones intercalate; with B2, B3, B5, and B6 electrofacies where sandstones and shales intercalate; and, with B6, B7, and B9 electrofacies where sandstones are intercalated to diamictite or, next to them.

The B9 electrofacies presents the lowest \underline{GR} values (~ 21 API) and \underline{RHOB} values like those of B8 electrofacies. The mean porosity values for electrofacies B9 are slightly lower than those of the previous electrofacies, being $\underline{NPHI} < \underline{\phi_{e_{ND}}}$. This factor is probably related to the shale

content of the electrofacies, since its almost entirely related to low GR sandstones (99% of the samples). In the RC1 model, the records are mainly below 2700 m in depth, in sections of sandstone adjacent to diamictite, where B9 electrofacies is commonly associated with B7 and B8 electrofacies. In RC2 model, the records extent to a broader range (2520 and 3074 m in depth) of sandstone sections. In this case, electrofacies B9 commonly associates with electrofacies B8.

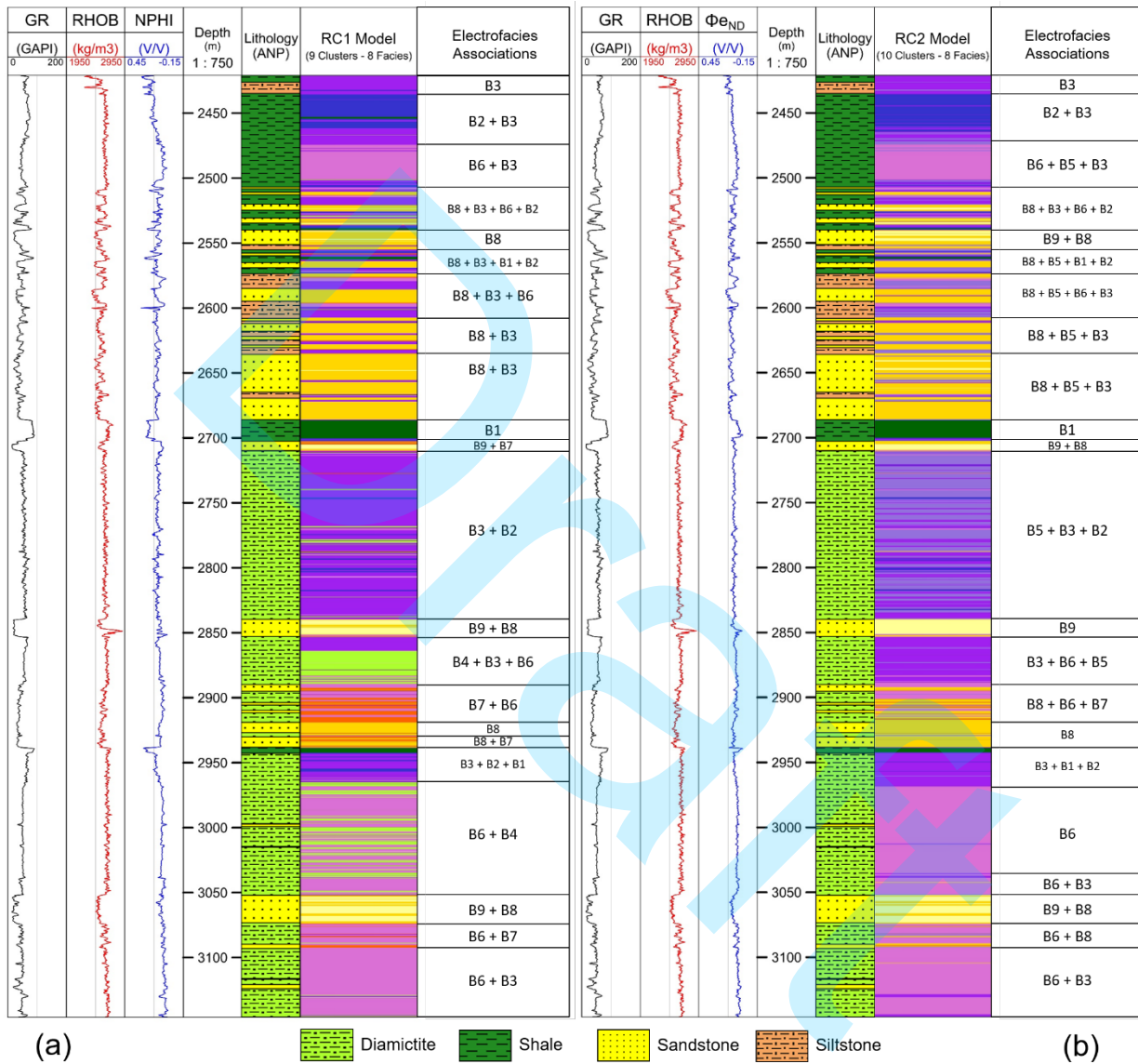


Figure 7 – Models determined for 1RCH-1-SC well based on the neutron porosity log (a), and effective porosity determined by the neutron-density method (b).

The RC1 and RC1 models also comprise electrofacies in which the elements assigned to the diamictites interval predominate, followed by the sandstone interval. Despite this condition, the RC1 and RC2 models received, proportionally, greater contributions of elements assigned to the shale and siltstone intervals than the models generated for 1GO-1-SC well.

CONCLUSIONS

In this study, a new workflow was used for electrofacies modeling, incorporating geophysical and geological information from two wells in the Itararé Group (Paraná Basin). Shale volume (V_{sh}) and effective porosity (Φ_e) were determined and partially applied as petrophysical input parameters and helped to achieve an excellent correspondence between geological and petrophysical parameters. The main findings are presented below:

- (1) The petrophysical parameters of volume shale (V_{sh}) and effective porosity (Φ_e) were determined using different methodologies, which allowed a comparative evaluation for each of these parameters. The results exhibit differences that may be associated to the method of calculation of these parameters and/or the lithologies involved. The electrofacies models were elaborated with distinct input parameters for each well (GO1, GO2, RC1 and RC2), so that it allowed to perceive heterogeneities within the lithologies of the wells, suggested by the way the electrofacies were recorded along the well and according to the chosen parameters in the modeling process.
- (2) The maximum, minimum and average values of V_{sh} from linear method (IGR) are overestimated in comparison to the non-linear method (Larionov Equation), mainly for the sandstone and shale intervals, where V_{sh} is lower and higher, respectively. The Φ_{eD} method in well 1RCH-1-SC returned low-precision results when compared to the Φ_{eND} method, specially to the sandstones interval (typical sandstone Φ_e values available in the literature are about 0.1 V/V for Itararé Group). The electrofacies models GO1 and GO2 suggest heterogeneities within the lithotypes of the analyzed wells: electrofacies A3, A4, A1, A2 and A5 for diamictite; and electrofacies A6, A7, A8, A9 and A10 for the sandstones. Shales are associated with electrofacies A1 and A2, while siltstones are associated with electrofacies A1, A2 and A4. The RC1 and RC2 models also indicate heterogeneities throughout the wells: i) electrofacies B2 and B3 are associated with the top shales of well 1RCH-1-SC, while the others with electrofacies B1; ii) electrofacies B3 and B5 (2,710 m), while the others are related to electrofacies B6 and B4; iii) B8 electrofacies is more related to sandstones, while electrofacies B7 occurs only in sandstones interbedded with diamictite and close to shales; iv) electrofacies B9 (sandstones) occurs below 2,700 m. Models RC1 and RC2 relate electrofacies B3, B5 or B6 to siltstones, however, they should not be considered representative only of this lithology, as they contribute only for 20% of the samples attributed to these electrofacies.
- (3) In the GO1 and GO2 models, MRGC modeling was efficient to determine diamictite and sandstone electrofacies. The GO1 model is relatively more accurate, considering diamictite and sandstone electrofacies, while the GO2 model was better for sandstones with low GR, associated to electrofacies A10. These models are efficient in determining

anomalous geophysical and petrophysical characteristics (electrofacies A2). In models RC1 and RC2, the electrofacies models were more efficient for diamictite, sandstone and shale. The RC1 and RC2 models present differences in the intervals with diamictite: i) the RC1 model recorded electrifications below 2,850 m, and ii) the RC2 model recorded more details in the diamictite.

(4) The sandstones of both wells presented mean porosity values (ϕ_{eD} and ϕ_{eND}) that range from 0.077 to 0.101 V/V, which corroborate previous works in the Itararé Group, such as França & Potter (1989, 1991). Nonetheless, it is important to highlight that, specifically for the 1RCH-1-SC well, the ϕ_{eD} value for sandstones is much higher than ϕ_{eND} (almost two times), which was one of the reasons for not using Φ_{eD} as an input log/parameter in the electrofacies-modeling of this well.

ACKNOWLEDGMENTS

This work was supported by the “*Técnicas Machine Learning para Reconhecimento de Padrões Sedimentológicos de Sistemas Turbidíticos - MLTurb*” project funded by PETROBRAS. The authors also thank to the Brazilian National Agency of Petroleum, Natural Gas and Biofuels (ANP) to provide the geophysical data, and to Emerson for training and GEOLOG software license.

REFERENCES

- Almeida, F.F.M., Hasui, Y., Brito Neves, B.B, Fuck, R.A, 1977, *Províncias Estruturais Brasileiras*. VIII Simpósio de Geologia do Nordeste, Campina Grande, Atas, Sociedade Brasileira de Geologia, p. 363-391.
- Asquith, G., & Gibson, C.R, 1982, *Basic Well Log Analysis for Geologists*: Tulsa, OK, USA: AAPG, Methods in Exploration Series, n. 3, 216 pp. <https://doi.org/10.1306/Mth3425>.
- Asquith, G., Krygowski, D., Henderson, S., Hurley, N, 2004, *Basic Well Log Analysis*: Tulsa, OK, USA: Methods in Exploration 16 (AAPG), 244 pp. <https://doi.org/10.1306/Mth16823>.
- Bateman, R.M., & Konen, C.E, 1977, *The Log Analyst and the Programmable Pocket Calculator: Part II – Crossplot Porosity and Water Saturation*. *The Log Analyst*, 18(5):3-11.
- Bocardi, L.B., Fernandes, L.A., Rostirolla, S.D., Appi, C.J, 2006, *Diagênese dos Arenitos do Grupo Itararé, Permocarbonífero, Bacia do Paraná*. *Revista Brasileira de Geociências*, 36(2):221-231. <https://doi.org/https://doi.org/10.25249/0375-7536.2006362221231>.
- Buso, V.V., Aquino, C.D., Paim, P.S.G., Mori, A.L., Fallgatter, C., Milana, J.P., Kneller, B, 2019, *Late Palaeozoic Glacial Cycles and Subcycles in Western Gondwana: Correlation of Surface and Subsurface Data of the Paraná Basin, Brazil*. *Palaeogeography, Palaeoclimatology, Palaeoecology*, 531. <https://doi.org/10.1016/j.palaeo.2017.09.004>.
- Eyles, C.H., Eyles, N., França, A.B, 1993, *Glaciation and Tectonics in an Active Intracratonic Basin: the Late Palaeozoic Itararé Group, Paraná Basin, Brazil*. *Sedimentology*, 40:1-25.

<https://doi.org/10.1111/j.1365-3091.1993.tb01087.x>

França, A.B., 1987, Stratigraphy, Depositional Environment and Reservoir Analysis of the Itararé Group (Permo-Carboniferous), Paraná Basin, Brazil. PhD Thesis. University of Cincinnati, Cincinnati, Ohio, USA.

França, A.B., & Potter, P.E., 1988, Estratigrafia, Ambiente Depositional e Análise de Reservatório do Grupo Itararé (Permocarbonífero), Bacia do Paraná (Parte 1). Boletim de Geociências da Petrobras, 2(2-4):147-191.

França, A.B., & Potter, P.E., 1989, Estratigrafia, Ambiente Depositional do Grupo Itararé (Permocarbonífero), Bacia do Paraná (Parte 2). Boletim de Geociências da Petrobras, 3:17-28.

França, A.B., & Potter, P.E., 1991, Stratigraphy and Reservoir Potential of Glacial Deposits of the Itararé Group (Permo-Carboniferous), Paraná Basin, Brazil. Bull. Am. Ass. Petrol. Geol., 75:62-85.

Larionov, V.V., 1969, Borehole Radiometry: Nedra, Moscow, Russia.

Malone, S.J., Meert, J.G., Banerjee, D.M., Pandit, M.K., Tamrat, E., Kamenov, G.D., Pradhan, V.R., Sohl, L.E., 2008. Paleomagnetism and Detrital Zircon Geochronology of the Upper Vindhyan Sequence, Son Valley and Rajasthan, India: A ca. 1000 Ma Closure age for the Purana Basins? Precambrian Research 164, 137–159. <https://doi.org/10.1016/j.precamres.2008.04.004>.

Milani, E.J., França, A.B., Schneider, R.L., 1994, Bacia do Paraná. Boletim de Geociências – Petrobras, 8(1):69-82.

Milani, E. J. Comentários sobre a origem e a evolução tectônica da Bacia do Paraná. In: Mantesso-Neto V., Bartorelli, A., Carneiro, C.D.R., Brito Neves, B.B. Geologia do Continente Sul-Americano: Evolução da obra de Fernando Flávio Marques de Almeida. São Paulo: Beca, 2004. p. 239-265

Milani, E.J., Melo, J.H.G., Souza, P.A., Fernandes, L.A., França, A.B., 2007, Bacia do Paraná. Boletim de Geociências – Petrobras, 15(2):265-287.

Meert, J.G., Pandit, M.K., Pradhan, V.R., Banks, J., Sirianni, R., Stroud, M., Newstead, B., Gifford, J., 2010, Precambrian crustal evolution of Peninsular India: a 3.0 billion year odyssey. Journal of Asian Earth Sciences 39, 483–515. <https://doi.org/10.1016/j.jseaes.2010.04.026>.

Sagar, B.S.D., Cheng, Q., Agterberg, F., 2018, Handbook of Mathematical Geosciences: Fifty Years of IAMG. Gewerbestrasse, Cham, Switzerland: Springer International Publishing, 914 pp.

Serra, O., & Abbott, H.T., 1982, The Contribution of Logging Data to Sedimentology and Stratigraphy. Society of Petroleum Engineers Journal, 22(1):117-131. <https://doi.org/10.2118/9270-PA>.

Ye, S.J., & Rabiller, P., 2000, A New Tool for Electro-Facies Analysis: Multi-Resolution Graph-Based Clustering. SPWLA 41st Annual Logging Symposium, Dallas, Texas, USA, 4-7 June 2000.

Ye, S.J., & Rabiller, P., 2005, Automated Electrofacies Ordering. Petrophysics, 46(6):409-423.

Almeida, M. A.: Conceptualization of the research. Data request, database structuring, data evaluation and data processing. Calculation of Petrophysical Parameters and Electrofacies Determination. Analysis,

evaluation, and interpretation of the Results. Image Preparation. Writing; **Nascimento, M. S.:** Conceptualization of the research. Supervision of all stages of the research as a Master's Degree Advisor. Writing; **Mota Alves, M. F.:** Data evaluation and data processing: analysis, preparation and interpretation of Density Logs (RHOB) data. Image Preparation.

Draft